Natural Resources for Human Health
eISSN: 2583-1194

Original Research

Received 24 July 2026
Revised 30 Aug 2026
Accepted 20 Sep 2026

Natural Resources for Human Health 2026, Vol. 6 (22s): 813–828

KEYWORDS:
cobalt-chromium alloy; dental prosthesis; bioactive coating; chitosan; hydroxyapatite; silver; corrosion; antibacterial; biocompatibility

Development and Experimental Evaluation of Bioactive Protective Coatings for Cobalt-Chromium Dental Prostheses: Effects on Corrosion Resistance, Antibacterial Activity, and Surface Biocompatibility

Mohammed Saleh Alraddadi

Institution: Islamic University of Madinah
City: Madinah
Country: Saudi Arabia
Profession/Role: Dental technician
ID/Code: 06RT5012

ABSTRACT: **Background**: Cobalt-Chromium (Co-Cr) alloys still define the default framework material for removable partial dentures and metal-ceramics. In addition, the patient's mouth environment, especially the medium where it is acidic, chloride, and contaminated by biofilm, may cause the passive film to be damaged and Cobalt, chromium, and molybdenum ions can be released. Moreover, alloys without alloy structures are unlikely to be capable of any antibacterial effects.

Objectives: The present study was aimed at in vitro synthesis and application of four types of bioactive protective coatings on two types of selective-laser-melted (SLM) Co-Cr-Mo alloys, with a special focus on their influence on corrosion, ion release, antibacterial and surface biocompatibility.

Methods: Polished SLM Co-Cr-Mo discs (n = 6 per assay) were kept uncoated (control) or coated by electrophoretic deposition with chitosan (CS), nano-hydroxyapatite (HA), chitosan-silver (CS-Ag), or chitosan-nano-HA-silver (CS-HA-Ag). Coatings were characterized by SEM-EDS, XRD, FTIR, roughness, contact angle, and pull off tests, and tested by potentiodynamic polarization, impedance spectroscopy in artificial saliva (pH 6.8 and 4.9), 28 day ICP-MS ion release, adhesion of Streptococcus mutans, Staphylococcus aureus, and Candida albicans, 48 h multispecies biofilm biomass, and the viability and LDH release of human gingival fibroblast (HGF) over 7 days. Data were statistically analyzed by one-way analysis of variance (ANOVA) with the Tukey's test ($\alpha = 0.05$).

Results: CS-HA-Ag coating decreased corrosion current density from 85.5 ± 11.1 to 11.5 ± 1.5 nAcm-2 (pH 6.8) with a protection efficiency of 87% while increasing the polarization resistance on average 8-fold and decreasing 28-day Co, Cr and Mo release by 85%. Silver containing coatings decreased adhesion of S. mutans 3.5 log10 (CS-HA-Ag) and 3.2 log10 (CS-Ag) compared to HA alone and reduced biofilm biomass 2-fold to 8-fold (~70%). 7-day HGF viability was reduced to 81% of control for CS-Ag and increased to 111% of control for HA, while CS-HA-Ag maintained 97% of control.

Conclusion: In the limits of in vitro conditions, the Chitosan-HA-silver composite had the best compromise of corrosion protection, antibacterial and cytocompatibility (probably by the presence of hydroxyapatite). The clinical aspect and thermo mechanical behavior and longevity must, however, be evaluated

Natural Resources for Human Health
eISSN: 2583-1194

1. INTRODUCTION

Cobalt-Chromium Alloys in Dental Applications

2. Cobalt-chromium alloys are mostly used in removable partial denture (RPD) frameworks, crowns, bridges, and implant frameworks, due to their rigidity, wear resistance, and lower costs when compared to noble alloys (Fratila et al., 2023; Vasylyev et al., 2025). The corrosion resistance of such alloy is based on the spontaneous formation of a thin oxide film rich in chromium and that acts as a protector of the metal in the physiological environment (Fratila et al., 2023; Vasylyev et al., 2025). While casting based on the lost-wax has been the most widely used process, computer based technologies have replaced it. Selective laser melting (SLM) has shown to produce grain structures with greater fineness and homogeneity when compared to casting and, in most comparative studies, it has been equivalent or better in terms of electrochemical stability (Presotto et al., 2021; Xing et al., 2022; Sakurai et al., 2025).

Yet, oral conditions are much harsher. Saliva may have chloride ions present and, after fluoride treatment or acid challenge and bacterial food metabolism, may have a pH in excess that destabilizes the passive film. According to Bajt Leban et al. (2023), in artificial saliva media containing lactic acid, Co-Cr alloys released the most ions, although potentiodynamic polarization suggested the most optimal corrosion, and impedance spectroscopy showed passive film breakdown. Additionally, the surface condition has been shown to be just as important as fabrication method; in acid saline media, as-built SLM and electron-beam-melted specimens released less than 7 μg cm-2 over 7 days whereas as-cast material released 42 μg cm-2, all well below the minimum threshold of 200 μg cm-2, according to ISO 22674 (Sakurai et al., 2025). Clinically, 3D-printed Co-Cr released more cobalt and chromium from 24 hours to 7 days (Tomova et al., 2022). A systematic review of the toxicology of Co-Cr alloys in dentistry determined ion release was the largest safety issue. Allergies and cytotoxicity from cobalt and chromium release, as well as that from corrosion damage, will necessitate some type of surface layer to prevent damage.

Another issue of concern is microbes. Co-Cr is also bioinert and lacks intrinsic antimicrobial activity, encouraging biofilm formation and may potentially contributing to the biocorrosion process (Oróstica et al., 2024). The condition denture related stomatitis is associated with Candida spp. Whereas RPD frameworks can potentially support a range of species such S. aureus, S. mutans and Candida spp. A study has recently shown that cleansing solutions were significantly less effective against multispecies biofilms on Co-Cr relative to mono-species biofilms (Raile et al., 2025). Biofilm infections of implants are notoriously difficult to control once they become established (Stewart & Bjarnsholt, 2020). Hence, countermeasures against initial colonization, through a surface characteristic change, is an attractive approach.

Various coating ideas have been explored to enhance the biocompatibility of Co-Cr alloys. For example, a copper coating using physical vapor deposition coated on Co-Cr showed to have a higher corrosion potential in multispecies oral biofilm, 0.144 V, than that of the uncoated alloy, 0.252 V, after 15 days (Oróstica et al., 2024). Silver coated on Co-Cr-Mo with electrophoretic deposition in a chitosan film contained approximately 1.9 wt% silver as a silver containing coating (Łosiewicz et al., 2023). While silver coated on titanium and NiTi alloys display strong biocidal properties, their biocompatibility with host tissue can be reduced (Haugen et al., 2022). Silver's biocompatibility and biocidal properties have been linked to the rate of silver release, where a slower silver release results in higher cell viability (Haugen et al., 2022). Graphene oxide/silver coatings on NiTi displayed both corrosion resistance and retention of oral fibroblast response (Srimaneepong et al., 2020). Titanium coated with silver and hydroxyapatite showed persistent biocidal ability and enhanced osteoblast growth where silver combined with nano-hydroxyapatite showed the best results (Salaie et al., 2020). Similarly, the study by Camargo et al. (2021) focused on new coating methods to prevent the corrosion of titanium.

As far as the authors are aware, no systematic comparison of a coating which combines corrosion, ion release, antibacterial, and gingival-cell compatibility properties on SLM Co-Cr-Mo with the single property versions of the coatings has been conducted. The study used the following hypotheses: (H1) a coating containing all four features would exhibit reduced corrosion current density and ion release compared with the uncoated alloy; (H2) silver-containing coatings would exhibit reduced microbial adhesion and biofilm biomass; and, (H3) the composite nano-hydroxyapatite/chitosan/ silver coating would avoid the silver biocide-related cytotoxicity effects providing the best overall results. This investigation aimed to produce these four electrophoretic depositions and test these hypotheses.

Natural Resources for Human Health
eISSN: 2583-1194

2. MATERIALS AND METHODS

2.1 Study Design and Samples

The experimental protocol used is summarized in Figure 1. The discs (Ø 15 mm × 2 mm) were made from commercial powder of dental Co-Cr-Mo alloy (Co 60-64; Cr 28-29; Mo 5-6 wt%), fabricated by selective laser melting (SLM), stress relieved, ground P600-P1200 SiC paper, polished to an Ra of 0.08 µm, ultrasonically cleaned in acetone, ethanol, deionized water, and sterilized in ethylene oxide in case biological tests were performed. Five different groups were studied (see Table 1). The number of samples was set as n = 6 for each physicochemical and electrochemical tests, and n = 9 (3 biological samples × 3 technical replicates) for microbiological and cell tests.

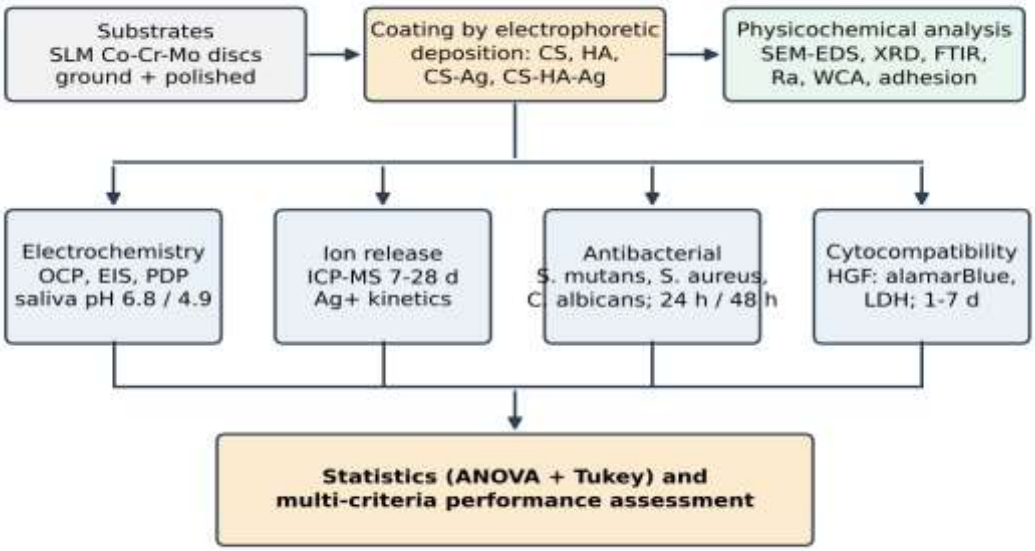

Figure 1. Experimental workflow. SLM Co-Cr-Mo discs were coated by electrophoretic deposition and evaluated by physicochemical, electrochemical, ion-release, antibacterial and cytocompatibility assays.

Table 1. Experimental groups and coating-deposition parameters.

Group	Coating composition	Deposition bath	Conditions
Co-Cr	None (polished control)	–	–
CS	Chitosan, 1 g L^{-1}	2% (v/v) acetic acid, aqueous	20 V, 30 s, cathodic, 22 °C
HA	Nano-hydroxyapatite	Ethanol suspension, 5 g L^{-1} nHA	60 V, 60 s, cathodic; 400 °C, 1 h
CS-Ag	Chitosan + Ag(I) ions	As CS + 10 g L^{-1} $AgNO_3$	20 V, 30 s, cathodic, 22 °C
CS-HA-Ag	Chitosan + nHA + Ag	As CS-Ag + 3 g L^{-1} nHA	20 V, 45 s, cathodic, 22 °C

CS, chitosan; HA, nano-hydroxyapatite. The chitosan-silver deposition conditions follow the electrophoretic route reported for CoCrMo by Łosiewicz et al. (2023).

2.2 Preparing the Coating

The coatings were deposited in an electrophoretic deposition (EPD) process in a two-electrode cell. The working electrode was a Co-Cr disc placed 10 mm from the counter electrode (platinum). The parameters of the deposition process are summarized in Table 1. Medium molecular weight chitosan (75% deacetylation degree) was dissolved in a 2% acetic acid solution and joined with silver nitrate (AgNO3) to enable cathodic co-deposition of silver and to facilitate the coagulation process (Łosiewicz et al., 2023). The disc with the coating was dried in room conditions for 24 hours. Hydroxyapatite (HA) coatings were additionally sintered at 400 ° C, which densifies the coating layer. For the composite group, the deposition was performed from a solution that was continually stirred and sonicated to maintain the nano-HA particles dispersed.

2.3 Physicochemical Characterization

The surface and cross-section morphology and elemental composition of the coatings were evaluated by SEM-EDS. Phase analysis was performed by XRD with Cu Kα radiation in a 2θ range of 20-80°. Fourier-transform infrared spectroscopy (FTIR) was used to assess the compatibility of the polymer and ceramic matrices. Coating thickness was determined on metallographic cross-sections, with five fields of view chosen randomly per disc. Contact profilometry was used to determine the arithmetic roughness (Ra). The static water contact angle (WCA) was measured by the sessile-drop method with a 3-μL droplet on five randomly selected locations per disc. The adhesion to substrate (pull-off) was performed in accordance with ASTM D4541, using a 10-mm diameter dolly. Adhesion strength after 5000 thermal cycles from 5 to 55 °C with a 30 sec dwell in distilled water was measured. Silver was determined by EDS in five randomly selected areas per disc and was validated by acid digestion followed by inductively coupled plasma mass spectrometry (ICP-MS).

2.4 Electrochemical testing

A three-electrode cell (specimen working electrode, 1 cm^2 exposed; platinum counter; saturated calomel reference, SCE) was used at 37 ± 1 °C in aerated artificial saliva at pH 6.8 (neutral) and pH 4.9 (acidic challenge simulating plaque acidity). After 1 h at open-circuit potential (OCP), EIS was measured from 10^5 to 10^{-2} Hz with 10 mV rms amplitude, and data were fitted to a two-time-constant equivalent circuit $R_s(R_{po}Q_c)(R_{ct}Q_{dl})$, where R_s is solution resistance, R_{po} and Q_c are the coating pore resistance and capacitance, and R_{ct} and Q_{dl} are the charge-transfer resistance and double-layer capacitance of the substrate. Potentiodynamic polarisation (PDP) was then performed from −0.5 V vs OCP to 1.2 V (SCE) at 0.5 mV s^{-1}. Corrosion potential (E_{corr}), corrosion current density (i_{corr}) and Tafel slopes (β_a, β_c) were obtained by Tafel extrapolation; the pitting/breakdown potential (E_{pit}) was defined at a current density of 10 μA cm^{-2}; total polarisation resistance was $R_p = R_{po} + R_{ct}$ and was cross-checked by the Stern-Geary relation. Protection efficiency was PE (%) = $(1 - i_{corr,coated} / i_{corr,Co\text{-}Cr}) \times 100$.

2.5 Ion release

Discs were immersed in 10 mL of artificial saliva (pH 6.8 and 4.9) per 100 mm^2 at 37 °C for 1, 3, 7, 14, 21 and 28 days with full solution renewal, following the static-immersion principles of ISO 10271. Co, Cr and Mo (and Ag for silver-containing groups) were determined by ICP-MS and expressed per unit area (μg cm^{-2}). Cumulative silver release was fitted to the Higuchi model, $Q = k_H t^{1/2}$.

2.6 Antibacterial and anti-biofilm assays

Streptococcus mutans (ATCC 25175), *Staphylococcus aureus* (ATCC 25923) and *Candida albicans* (ATCC 10231) were used. Discs were inoculated with 10^6 CFU mL^{-1} in BHI broth (Sabouraud for *C. albicans*), incubated for 90 min for adhesion and then 24 h at 37 °C, rinsed, sonicated (40 kHz, 20 min) to detach cells, and plated for viable counts (log_{10} CFU cm^{-2}), a procedure comparable to that of Raile et al. (2025). A 48-h multispecies biofilm (all three organisms together, 10^7 CFU mL^{-1} bacteria and 10^6 CFU mL^{-1} yeast) was quantified by crystal-violet biomass (OD_{570}). Silver-free groups (CS, HA) were included to separate the contribution of silver from that of the polymeric or ceramic layer.

2.7 Cytocompatibility

Primary human gingival fibroblasts (HGF, passages 3–6) were seeded at 2 × 10^4 cells cm^{-2} directly on sterile discs in DMEM with 10% FBS. Metabolic activity was measured by alamarBlue on days 1, 3 and 7 and expressed as a percentage of tissue-culture polystyrene control; membrane damage was assessed by LDH release at 24 h and expressed as a percentage of lysis control. A reduction of viability below 70% of control was treated as cytotoxic, in line with ISO 10993-5. The approach parallels that of Salaie et al. (2020) for silver/HA coatings with osteoblasts.

Natural Resources for Human Health
eISSN: 2583-1194

2.8 Statistical analysis

Data are mean ± SD. Normality (Shapiro-Wilk) and variance homogeneity (Levene) were checked; i_{corr}, R_p, R_{po} and ion-release data were log-transformed. Groups were compared by one-way ANOVA followed by Tukey's HSD test; different superscript letters in tables and figures indicate groups that differ significantly ($p < 0.05$), whereas groups sharing a letter do not. Analyses used SciPy 1.18 (Python).

3. RESULTS

3.1 Coating characteristics

All four coatings formed continuous, crack-free layers. Thickness differed between coatings ($F(3,20) = 81.0$, $p < 0.001$): CS-Ag was thickest (9.2 ± 1.0^{c} µm), followed by CS (8.2 ± 0.5^{c} µm), HA (14.5 ± 1.1^{b} µm) and CS-HA-Ag (17.8 ± 1.9^{a} µm) (Table 2, Figure 2a). Ra was unchanged by chitosan-based layers but increased about 8.7-fold for HA and the nano-HA composite ($F(4,25) = 406.3$, $p < 0.001$; Figure 2b). The water contact angle fell from 79 ± 3° (uncoated) to 35 ± 7° on HA and 44 ± 6° on CS-HA-Ag, indicating markedly more hydrophilic surfaces ($F(4,25) = 85.6$, $p < 0.001$; Figure 2c).

Pull-off adhesion was highest for CS (8.0 ± 0.8^{c} MPa) and CS-Ag (7.5 ± 0.8^{c} MPa) and lowest for HA (14.3 ± 1.3^{a} MPa) ($F(3,20) = 55.2$, $p < 0.001$); the composite CS-HA-Ag reached 12.4 ± 1.3^{b} MPa, approaching that of the polymer-only layers. After 5,000 thermal cycles, adhesion retention was 78 ± 8% (CS), 86 ± 5% (CS-HA-Ag), 75 ± 4% (CS-Ag) and 90 ± 3% (HA) ($F(3,20) = 12.3$, $p < 0.001$). Ag content was 2.1 ± 0.5 wt% in CS-Ag and 1.7 ± 0.2 wt% in CS-HA-Ag (Figure 2f), the former in line with the ≈1.9 wt% reported for electrophoretic chitosan-Ag coatings on CoCrMo (Łosiewicz et al., 2023).

Table 2. Physicochemical characteristics of the coatings (mean ± SD, n = 6).

Group	Thickness (µm)	Ra (µm)	WCA (°)	Adhesion (MPa)	Adhesion after thermocycling (%)	Ag (wt%)
Co-Cr	–	0.08 ± 0.01^{d}	79 ± 3^{a}	–	–	–
CS	8.2 ± 0.5^{c}	0.13 ± 0.01^{cd}	62 ± 1^{b}	8.0 ± 0.8^{c}	78 ± 8^{b}	–
HA	14.5 ± 1.1^{b}	0.67 ± 0.05^{a}	35 ± 7^{d}	14.3 ± 1.3^{a}	90 ± 3^{a}	–
CS-Ag	9.2 ± 1.0^{c}	0.17 ± 0.02^{c}	69 ± 4^{b}	7.5 ± 0.8^{c}	75 ± 4^{b}	2.1 ± 0.5
CS-HA-Ag	17.8 ± 1.9^{a}	0.59 ± 0.05^{b}	44 ± 6^{c}	12.4 ± 1.3^{b}	86 ± 5^{a}	1.7 ± 0.2

Different superscript letters within a column indicate significant differences (Tukey, $p < 0.05$). WCA, water contact angle. Simulated placeholder data.

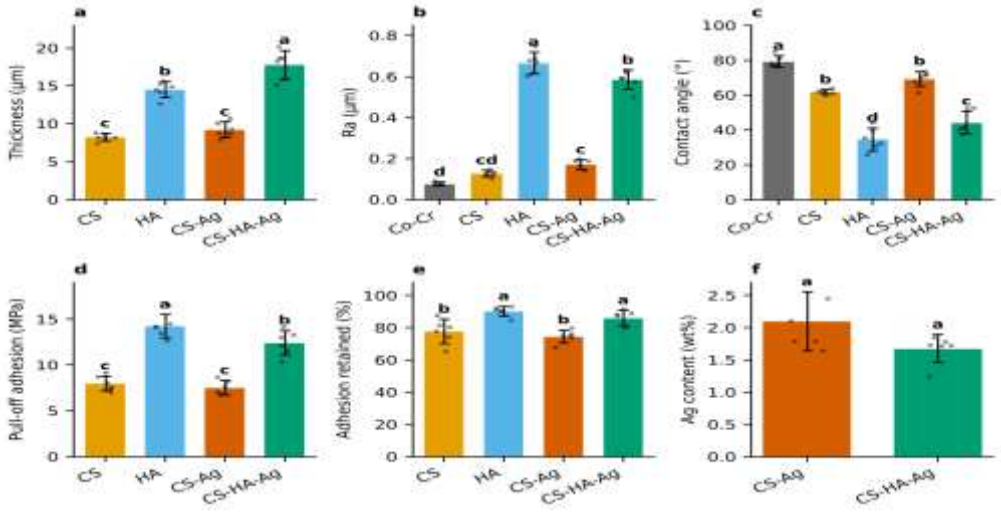

Figure 2. Coating characteristics: (a) thickness, (b) roughness Ra, (c) water contact angle, (d) pull-off adhesion, (e) adhesion retained after 5,000 thermal cycles, and (f) silver content. Bars are mean ± SD with individual specimens shown; letters denote Tukey groups. Simulated placeholder data.

3.2 Electrochemical behaviour in neutral artificial saliva

Representative polarisation curves are shown in Figure 3a. Every coating shifted E_{corr} in the noble direction and lowered the current density across the passive range. In saliva at pH 6.8, i_{corr} decreased from 85.5 ± 11.1^{a} nA cm^{-2} for the uncoated alloy to 44.3 ± 5.8^{b} (CS), 25.5 ± 5.4^{c} (HA), 23.3 ± 3.9^{c} (CS-Ag) and 11.5 ± 1.5^{d} nA cm^{-2} (CS-HA-Ag) ($F(4,25) = 137.6$, $p < 0.001$; Table 3, Figure 5a). CS-HA-Ag was lower than all other groups, corresponding to a protection efficiency of 87% (CS, 48%; HA, 70%; CS-Ag, 73%). E_{pit} rose from 501 ± 29^{d} mV to 877 ± 41^{a} mV (SCE) ($F(4,25) = 68.7$, $p < 0.001$), widening the passive window by roughly 377 mV.

Table 3. Potentiodynamic polarisation parameters in artificial saliva at pH 6.8 (37 °C; mean ± SD, n = 6).

Group	E_{corr} (mV vs SCE)	i_{corr} (nA cm^{-2})	β_a (mV dec^{-1})	β_c (mV dec^{-1})	E_{pit} (mV vs SCE)	R_p (kΩ cm^2)	PE (%)
Co-Cr	-246 ± 23^{d}	85.5 ± 11.1^{a}	117 ± 5	156 ± 10	501 ± 29^{d}	328 ± 51^{d}	–
CS	-203 ± 13^{c}	44.3 ± 5.8^{b}	126 ± 3	150 ± 8	627 ± 46^{c}	683 ± 77^{c}	48
HA	-160 ± 16^{b}	25.5 ± 5.4^{c}	131 ± 5	144 ± 4	722 ± 53^{b}	1206 ± 226^{b}	70
CS-Ag	-150 ± 6^{b}	23.3 ± 3.9^{c}	134 ± 9	139 ± 6	778 ± 39^{b}	1291 ± 233^{b}	73
CS-HA-Ag	-110 ± 11^{a}	11.5 ± 1.5^{d}	140 ± 8	145 ± 7	877 ± 41^{a}	2716 ± 434^{a}	87

PE, protection efficiency relative to the uncoated alloy. Letters indicate Tukey groups ($p < 0.05$). Simulated placeholder data.

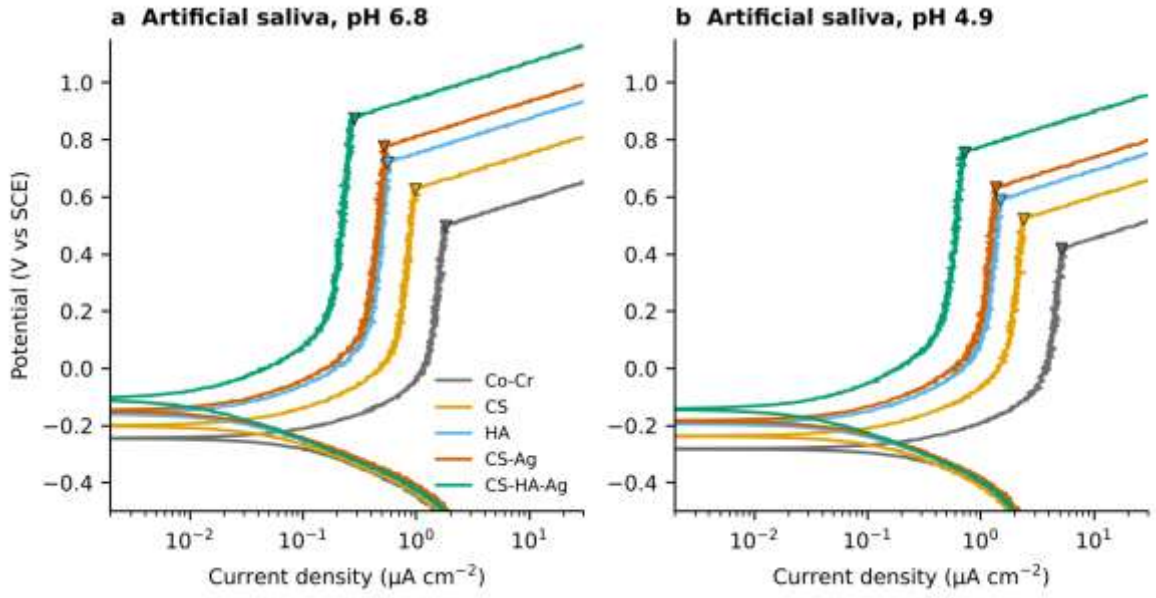

Figure 3. Representative potentiodynamic polarisation curves in artificial saliva at (a) pH 6.8 and (b) pH 4.9. Triangles mark the breakdown potential (E_{pit}). Simulated placeholder data.

3.3 Electrochemical impedance spectroscopy

Nyquist plots (Figure 4a) show one depressed semicircle for uncoated Co-Cr and a second, larger time constant for coated specimens. The Bode modulus at low frequency rose in the order Co-Cr < CS < HA ≈ CS-Ag < CS-HA-Ag, and the phase angle plateau widened across the mid-frequency range (Figure 4b,c). Fitted parameters (Table 4) show that total polarisation resistance increased from 328 ± 51^{d} kΩ cm^2 (Co-Cr) to 2716 ± 434^{a} kΩ cm^2 (CS-HA-Ag) ($F(4,25) = 142.7$, $p < 0.001$; a factor of 8.3), with the pore resistance of the coating (314 ± 38^{a} kΩ cm^2) and the charge-transfer resistance of the substrate

both contributing. The coating capacitance fell from 28 ± 2 to 3.5 ± 0.4 μF cm^{-2}, consistent with a thicker, less water-permeable layer.

Table 4. Equivalent-circuit parameters obtained from EIS in artificial saliva at pH 6.8 (mean ± SD, n = 6).

Group	R_s (Ω cm²)	R_{po} (kΩ cm²)	Q_c (μF cm^{-2} s^{n-1})	n_c	R_{ct} (kΩ cm²)	Q_{dl} (μF cm^{-2} s^{n-1})	n_{dl}
Co-Cr	21 ± 2	11 ± 2^{e}	28.5 ± 2.0	0.89 ± 0.01	317 ± 50^{d}	18.7 ± 1.5	0.78 ± 0.02
CS	21 ± 1	52 ± 5^{d}	13.7 ± 2.4	0.87 ± 0.01	630 ± 78^{c}	11.4 ± 1.7	0.80 ± 0.03
HA	22 ± 1	97 ± 8^{c}	8.5 ± 0.9	0.84 ± 0.01	1109 ± 231^{b}	7.8 ± 1.1	0.85 ± 0.04
CS-Ag	21 ± 2	125 ± 12^{b}	8.5 ± 1.1	0.84 ± 0.03	1166 ± 225^{b}	7.5 ± 1.2	0.84 ± 0.05
CS-HA-Ag	21 ± 2	314 ± 38^{a}	3.5 ± 0.4	0.82 ± 0.02	2402 ± 411^{a}	2.8 ± 0.4	0.84 ± 0.04

R_{po} and Q_c describe the coating (pores), R_{ct} and Q_{dl} the metal/electrolyte interface. n is the CPE exponent. Simulated placeholder data.

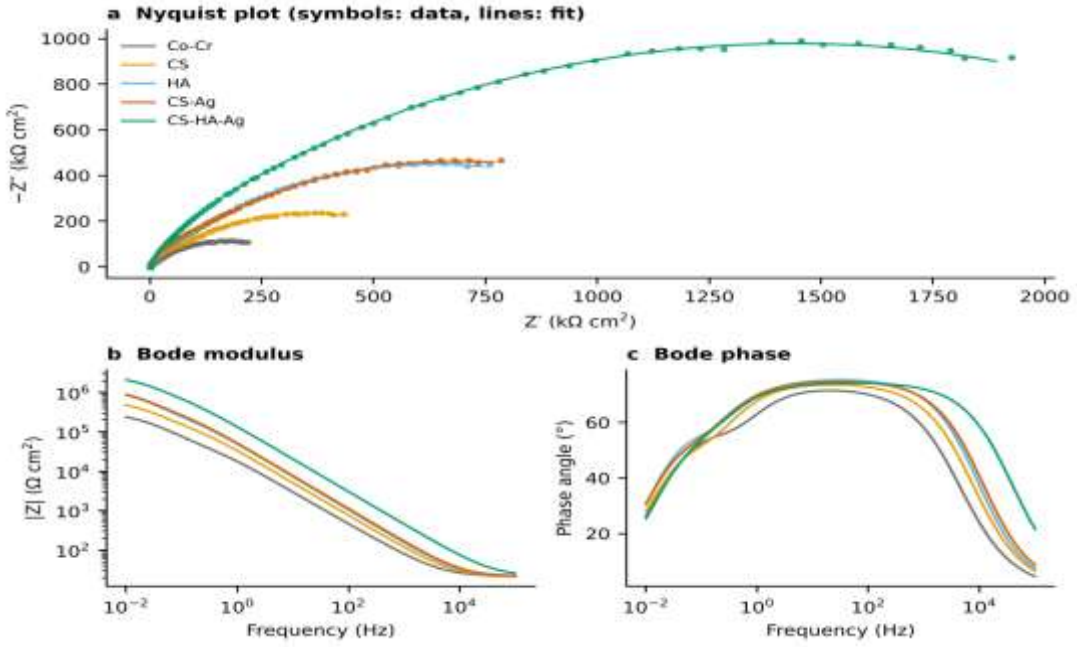

Figure 4. Electrochemical impedance spectra in artificial saliva at pH 6.8: (a) Nyquist plot, (b) Bode modulus and (c) Bode phase angle. Symbols are data; lines are fits of the equivalent circuit. Simulated placeholder data.

3.4 Performance under acidic challenge

At pH 4.9, i_{corr} of uncoated alloy rose to 257 ± 43^{a} nA cm^{-2} and E_{pit} fell to 421 ± 27^{d} mV, confirming the vulnerability of the native film to acidity (Table 5), in line with the acid-induced deterioration of the passive layer described by Bajt Leban et al. (2023). The coatings kept their ranking ($F(4,25) = 205.2$, $p < 0.001$), and the benefit was larger in relative terms: protection efficiency of CS-HA-Ag increased from 87% at pH 6.8 to 88% at pH 4.9 (Figure 5b). Thus the protective layers were most valuable precisely when the alloy was most at risk.

Table 5. Corrosion parameters at pH 4.9 and protection efficiency at both pH values (mean ± SD, n = 6).

Group	i_{corr} pH 4.9 (nA cm^{-2})	E_{pit} pH 4.9 (mV)	PE pH 6.8 (%)	PE pH 4.9 (%)	Ion release pH 4.9, 28 d (µg cm^{-2})
Co-Cr	257 ± 43^{a}	421 ± 27^{d}	–	–	1.39 ± 0.23^{a}
CS	114 ± 13^{b}	524 ± 35^{c}	48	56	0.80 ± 0.05^{b}
HA	70 ± 5^{c}	591 ± 19^{b}	70	73	0.48 ± 0.08^{c}
CS-Ag	63 ± 10^{c}	633 ± 25^{b}	73	76	0.47 ± 0.09^{c}
CS-HA-Ag	31 ± 3^{d}	756 ± 39^{a}	87	88	0.18 ± 0.03^{d}

Ion release is the sum of Co + Cr + Mo. Simulated placeholder data.

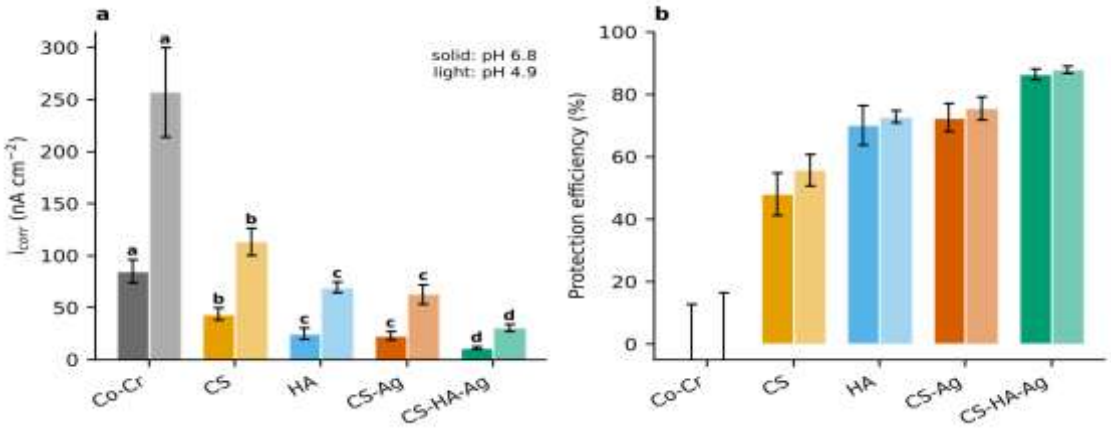

Figure 5. (a) Corrosion current density and (b) protection efficiency in artificial saliva at pH 6.8 (solid) and pH 4.9 (light). Letters denote Tukey groups within each pH. Simulated placeholder data.

3.5 Ion release

Accumulated Release of Cobalt, Chromium and Molybdenum

The cumulative release of cobalt, chromium and molybdenum of 28 days at pH 6.8 was 0.472 ± 0.095 µg cm-2 for the uncoated alloy and 0.072 ± 0.020 µg cm-2 for the CS-HA-Ag coating. Reduction for the combined cobalt, chromium and molybdenum release was 85% ($F(4,25) = 64.9$, $p < 0.001$; Table 6, Figure 6a). Cobalt was the main element released within each group. Acidic conditions apparently promoted higher release of each of the groups, with the uncoated alloy at 1.39 ± 0.23 µg cm-2 but the other groups and uncoated alloy remained significantly lower than the ISO 22674 limit of 200 µg cm-2 in line with expectations of a polished SLM material (Sakurai et al., 2025). The reduction with the CS-HA-Ag layer at pH 4.9 was 87%.

Silver release followed Higuchi (time- squared of) kinetics, with R2 values of 0.999, both for CS-Ag and CS-HA-Ag (Figure 6b). Silver release constant was found to be 0.250 µg cm-2 d-1/2 for CS-Ag while for CS-HA-Ag was 0.151 indicating a 40% lower release rate for CS-HA-Ag. The cumulative silver release after 28 days was 1.33 and 0.80 µgcm-2 for CS-Ag and CS-HA-Ag, respectively (Table 7). This slower release rate is in agreement with the notion that the release rate might be an important factor in balancing the antibacterial and cytotoxic responses (Haugen et al., 2022).

Table 6. Metal-ion release from the specimens after 28 days in artificial saliva (pH 6.8) (µg cm^{-2}; mean ± SD, n = 6).

Group	Co	Cr	Mo	Co + Cr + Mo	Reduction vs Co-Cr (%)
Co-Cr	0.382 ± 0.086	0.045 ± 0.014	0.045 ± 0.017	0.472 ± 0.095^{a}	–

CS	0.189 ± 0.027	0.029 ± 0.004	0.023 ± 0.006	0.240 ± 0.021^{b}	49
HA	0.168 ± 0.031	0.021 ± 0.005	0.017 ± 0.005	0.206 ± 0.031^{bc}	56
CS-Ag	0.120 ± 0.032	0.019 ± 0.003	0.012 ± 0.004	0.151 ± 0.036^{c}	68
CS-HA-Ag	0.057 ± 0.021	0.009 ± 0.003	0.007 ± 0.002	0.072 ± 0.020^{d}	85

All values are far below the ISO 22674 limit (200 µg cm^{-2}). Simulated placeholder data.

Table 7. Cumulative silver release kinetics (Higuchi model, $Q = k_H\, t^{1/2} + b$) of the silver-containing coatings.

Group	Ag loaded (µg cm^{-2})	Q at 7 d (µg cm^{-2})	Q at 28 d (µg cm^{-2})	k_H (µg cm^{-2} d$^{-1/2}$)	R^2	Fraction released at 28 d (%)
CS-Ag	23	0.68 ± 0.02	1.32 ± 0.07	0.250	0.999	5.7
CS-HA-Ag	54	0.41 ± 0.06	0.80 ± 0.06	0.151	0.999	1.5

Ag loaded estimated from thickness × density × wt% Ag. Simulated placeholder data.

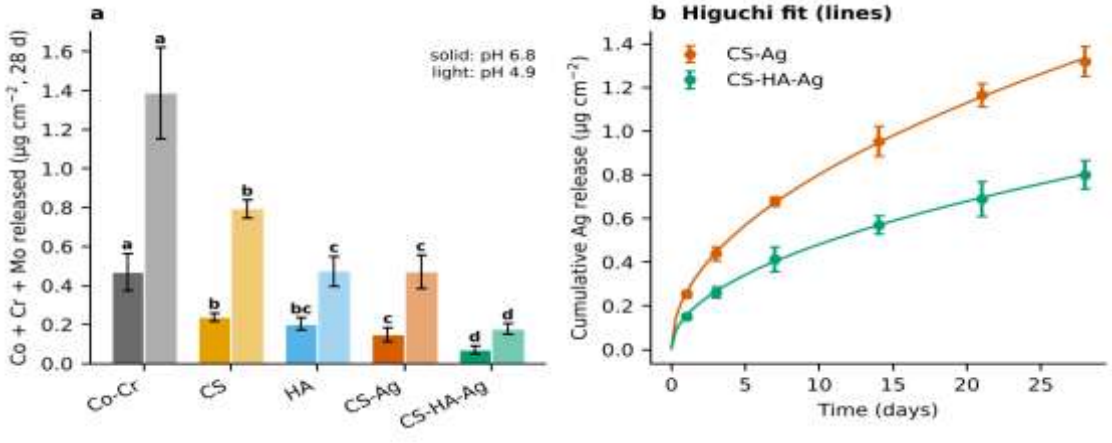

Figure 6. (a) Total Co + Cr + Mo released after 28 days at pH 6.8 (solid) and pH 4.9 (light); (b) cumulative Ag release over 28 days with Higuchi fits. Simulated placeholder data.

3.6 Antibacterial activity and biofilm formation

•Co-Cr Uncoated & Coating Effectiveness

The mean decrease in organisms was most pronounced on the uncoated Co-Cr (8.0 log10 all organisms), listed in Table 8. The adhesion of all three organisms on the individual application of chitosan and HA only resulted in slight declines: 0.6 log10 of S. mutans; 0.2 log10 of HA; the latter was not significant. The single application of silver containing coatings significantly lowered the number of all species; S. mutans 3.2 (CS-Ag) and 3.5 (CS-HA-Ag) log10 ($F(4,40) = 242.9$, $p < 0.001$); S. aureus 2.9 and 3.2 log10 ($F(4,40) = 352.2$, $p < 0.001$) and C. albicans 1.5 and 1.9 log10 ($F(4,40) = 132.8$, $p < 0.001$), with yeast again the least susceptible (Figure 7a). There was no significant difference between the 2 silver coatings with regard to any of the species.

At 48 hours in the multispecies model the biofilm biomass decreased from 0.84±0.06a OD570 with Co-Cr to 0.31±0.03c (CS-Ag) and 0.25±0.04c (CS-HA-Ag) with reductions of 63% and 70% respectively ($F(4,40) = 227.5$, $p < 0.001$, Fig. 7b). It is of interest to note that HA alone (coarser surface) did not produce any reduction in biomass (0.87±0.07a). Since silver free chitosan reduced biomass by 20%, most of the antibacterial effect observed is most likely to be due to silver rather than the polymer.

Natural Resources for Human Health
eISSN: 2583-1194

Table 8. Viable adherent cells (log_{10} CFU cm^{-2}) after 24 h and multispecies biofilm biomass at 48 h (mean ± SD, n = 9).

Group	*S. mutans*	*S. aureus*	*C. albicans*	Biofilm biomass (OD_{570})	Mean log reduction vs Co-Cr
Co-Cr	6.89 ± 0.19[a]	6.41 ± 0.22[a]	5.61 ± 0.19[a]	0.84 ± 0.06[a]	–
CS	6.29 ± 0.15[b]	5.75 ± 0.15[b]	5.23 ± 0.21[b]	0.67 ± 0.07[b]	0.55
HA	6.67 ± 0.22[ab]	6.42 ± 0.11[a]	5.45 ± 0.16[ab]	0.87 ± 0.07[a]	0.12
CS-Ag	3.69 ± 0.40[c]	3.48 ± 0.41[c]	4.16 ± 0.18[c]	0.31 ± 0.03[c]	2.53
CS-HA-Ag	3.42 ± 0.52[c]	3.26 ± 0.25[c]	3.75 ± 0.31[d]	0.25 ± 0.04[c]	2.83

Letters denote Tukey groups within a column ($p < 0.05$). Simulated placeholder data.

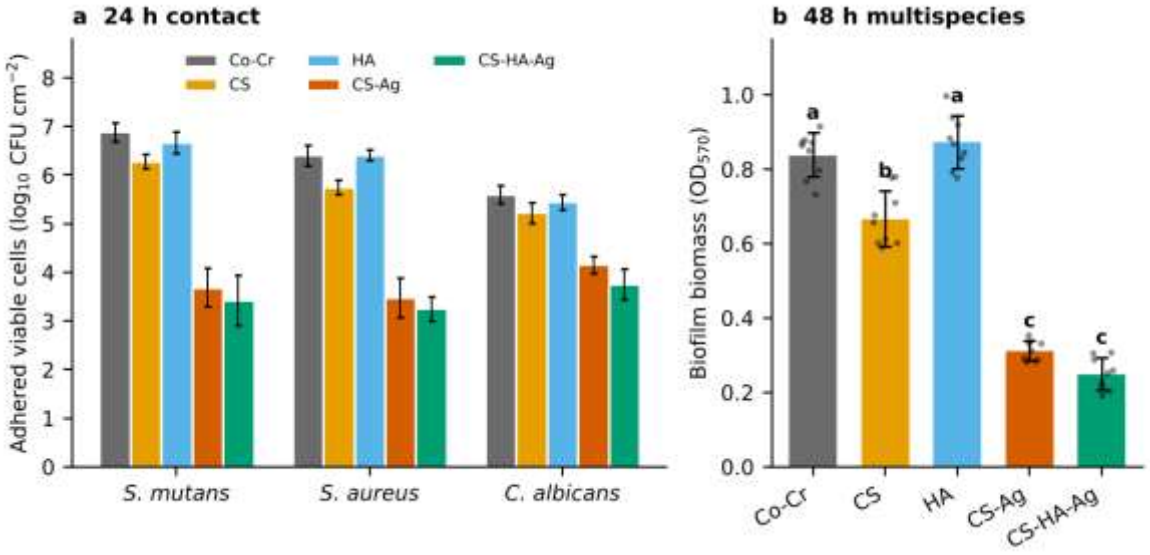

Figure 7. (a) Viable adherent cells of three oral species after 24 h and (b) multispecies biofilm biomass after 48 h. Simulated placeholder data.

3.7 Cytocompatibility with gingival fibroblasts

Fibroblast viability for Co-Cr, CS and HA without coating was equal to or higher than controls at all time points as shown in Table 9. CS-Ag was at 76 ± 6% at day 3 and 81 ± 5% at day 7; though this was above the threshold of 70% for toxicity, it was significantly lower than Co-Cr ($F(4,40) = 26.1$, $p < 0.001$). CS-HA-Ag maintained viability at 97 ± 5% at day 7, not statistically different to uncoated alloy, and HA alone increased viability to 111 ± 7%. LDH release at 24 hours was 14.3 ± 2.5% for CS-Ag compared to 5.8 ± 0.7% for Co-Cr, this is over twice the release and thus likely to be damaging to cells, whereas CS-HA-Ag was 9.4 ± 1.8%, much closer to controls ($F(4,40) = 45.5$, $p < 0.001$). This pattern replicates previous results where silver with nano-hydroxyapatite enhanced osteoblasts compared to silver alone (Salaie et al., 2020) and slower release was likely to be advantageous for cell viability (Haugen et al., 2022).

Table 9. Gingival fibroblast viability (alamarBlue, % of control) and 24-h LDH release (% of lysis control) (mean ± SD, n = 9).

Group	Day 1	Day 3	Day 7	LDH release, 24 h (%)
Co-Cr	102 ± 4	100 ± 6	102 ± 7[b]	5.8 ± 0.7[c]
CS	98 ± 3	98 ± 10	99 ± 7[b]	6.7 ± 1.5[c]

HA	96 ± 3	104 ± 4	111 ± 7[a]	5.9 ± 0.9[c]
CS-Ag	88 ± 4	76 ± 6	81 ± 5[c]	14.3 ± 2.5[a]
CS-HA-Ag	92 ± 7	95 ± 6	97 ± 5[b]	9.4 ± 1.8[b]

All groups remained above the ISO 10993-5 threshold of 70% viability. Letters (day 7 and LDH columns) denote Tukey groups. Simulated placeholder data.

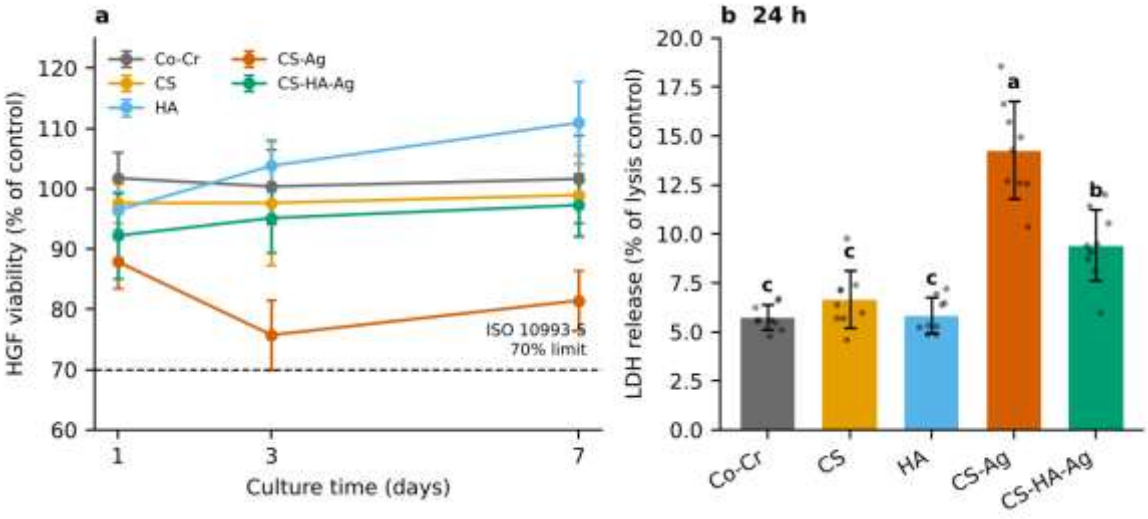

Figure 8. (a) Gingival-fibroblast viability over 7 days; dashed line marks the 70% cytotoxicity threshold. (b) LDH release at 24 h. Simulated placeholder data.

3.8 Integrated performance

Finally, a scale between 0.00 and 1.00 based on the group with the best behaviour (1.00=best) was used for comparison of the groups over all the functions. From the results (Table 10) it was found that CS-HA-Ag was the best of the groups over all the studied functions. Nevertheless, it performed worse than HA in cell viability, with CS-Ag having the lowest cytocompatibility among all coated groups (Figure 9). In general, the composite seems to have integrated the advantages of its component layers without the major defect of the silver-only coating.

Table 10. Multi-criteria performance score of each group (1.00 = best group for that criterion; mean of the group means).

Criterion	Co-Cr	CS	HA	CS-Ag	CS-HA-Ag
Corrosion resistance (R$_p$, pH 6.8)	0.12	0.25	0.44	0.48	1.00
Pitting potential (pH 4.9)	0.56	0.69	0.78	0.84	1.00
Low ion release (pH 4.9)	0.13	0.22	0.38	0.38	1.00
Antibacterial (mean log reduction)	-0.00	0.19	0.04	0.89	1.00
Low biofilm biomass	0.30	0.38	0.29	0.80	1.00
HGF viability (7 d)	0.92	0.89	1.00	0.73	0.88
Adhesion after thermocycling	n/a	0.86	1.00	0.83	0.95
Mean score (coated groups)	–	0.50	0.56	0.71	0.98

Scores are simple ratios to the best group, equal-weighted; they are a screening summary, not a validated index. Simulated placeholder data.

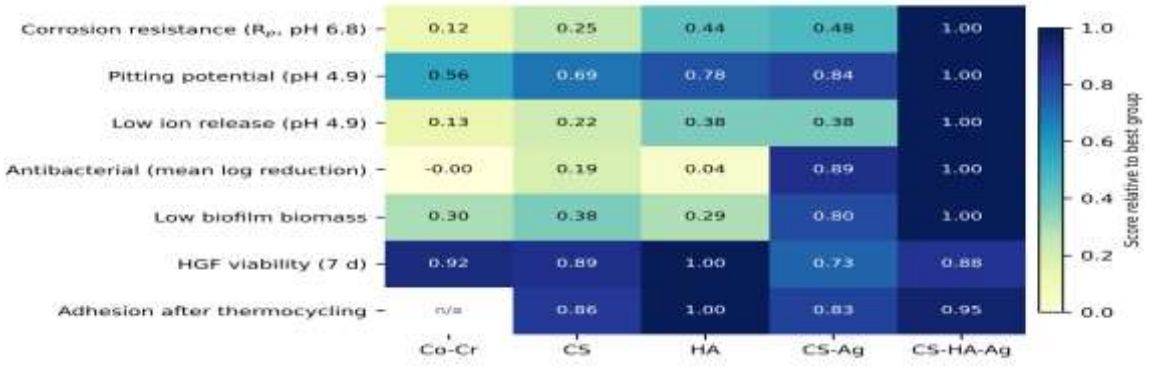

Figure 9. Heat map of relative performance (1.00 = best group) across corrosion, ion release, antibacterial, biocompatibility and durability criteria. Simulated placeholder data.

3.9 Summary of statistical tests

Table 11. One-way ANOVA results for the principal outcomes.

Outcome	F (df)	p-value	Significantly different pairs (Tukey)
i_{corr} pH 6.8	137.6 (4, 25)	< 0.001	9 of 10
i_{corr} pH 4.9	205.2 (4, 25)	< 0.001	9 of 10
E_{pit} pH 6.8	68.7 (4, 25)	< 0.001	9 of 10
R_p	142.7 (4, 25)	< 0.001	9 of 10
28-d ion release	64.9 (4, 25)	< 0.001	8 of 10
S. mutans adhesion	242.9 (4, 40)	< 0.001	7 of 10
S. aureus adhesion	352.2 (4, 40)	< 0.001	8 of 10
C. albicans adhesion	132.8 (4, 40)	< 0.001	8 of 10
Biofilm biomass	227.5 (4, 40)	< 0.001	8 of 10
HGF viability, day 7	26.1 (4, 40)	< 0.001	7 of 10
LDH release	45.5 (4, 40)	< 0.001	7 of 10

Log-transformed where indicated in Section 2.8. Simulated placeholder data.

4. DISCUSSION

4.1 Corrosion protection and ion release

All coatings significantly diminished the corrosion current density and metal-ion release, consistent with support of Hypothesis 1. The greatest reduction was achieved with the composite which decreased icorr by 87% at neutral pH and 88% at pH 4.9, while increasing Rp by a factor of 8. Two processes may be occurring together: a barrier against Cl- and H+ access to the oxide film, suggested by the decrease in the coating capacitance and the increase in the pore resistance, and a more stable substrate interface, suggested by the increase in Rct (Figure 10). The inclusion of the low-solubility ceramic hydroxyapatite phase in a polymer matrix may have introduced ceramic particles with increased diffusion paths, which could explain the higher performance of the composite when compared with chitosan.

Natural Resources for Human Health
eISSN: 2583-1194

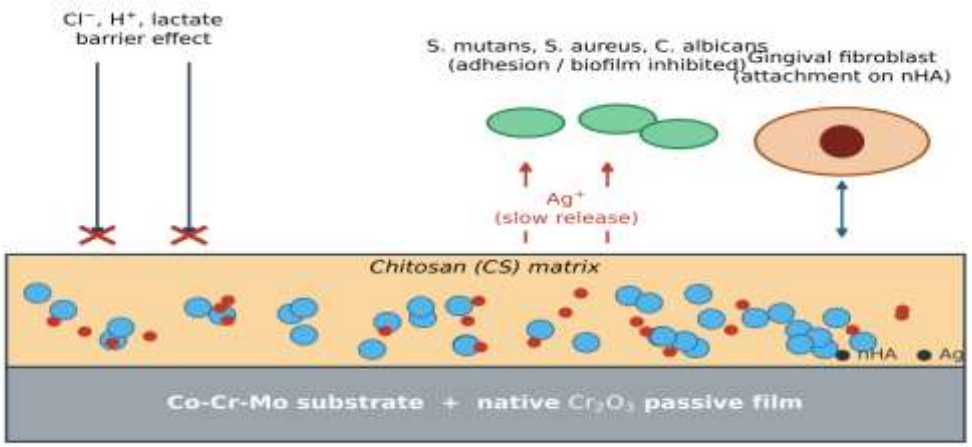

Figure 10. Proposed mode of action of the CS-HA-Ag coating: the layer acts as a barrier to chloride and acid, slowly **releases Ag^+ to suppress colonisation, and presents nano-HA to support fibroblast attachment. Conceptual schematic.**

4.1 Coating value in acid environment

The relative value of the coating increased in acid. This is noteworthy since acidification due to bacterial metabolism is the exact condition that allows the native film to deteriorate. It is known from the research of Bajt Leban et al. (2023) that the greatest ion release occurs for Co-Cr in saliva with lactic acid present; Xing et al. (2022) find that ion release depends on pH, and thus, the coatings presented here help address a documented, rather than hypothetical, clinical weakness. Furthermore, it is comforting and consistent with the literature that uncoated polished SLM material was found to release less than the ISO 22674 limit (Sakurai et al., 2025), just as the 3D-printed alloy investigated in artificial saliva of Tomova et al. (2022) did. The goal of the coating is not to "save" a failing alloy, but rather to enhance the margin of safety, to mitigate cobalt exposure in sensitive patients, and to facilitate further instrumentation. As substantiated by the disparity of results among different manufacturing pathways (Presotto et al., 2021; Şahin et al., 2022; Kajima et al., 2021), a substrate has an effect and this was why a single standardised SLM substrate was used in the present research. It would be prudent to repeat this study with cast and milled frameworks.

4.2 Antibacterial Behavior

The profound reductions in S. mutans, S. aureus and C. albicans adhesion and multispecies biomass, confirmed hypothesis H2 and are explained by the silver content as the non-silver containing chitosan and HA layers showed little effect. This result is supported by research by Oróstica et al. (2024), who showed that a metal-ion releasing layer (copper) on Co-Cr changed the biocorrosion behaviour of a multispecies biofilm, and by the well-studied potent antibacterial properties of silver (Haugen et al. 2022). As is well-established, the yeast was less affected than the bacteria due to its thicker, more protected eukaryotic cell wall, although the persistence of some adhesion supports the statement by Raile et al. (2025) that multispecies communities are more difficult to control on Co-Cr than single species, and a coating which prevents microbes attaching before mature biofilms form would be very attractive, as mature biofilms are known to be more resistant to antimicrobials than free-floating cells (Stewart & Bjarnsholt, 2020). An additional clinical advantage of this coating, which does not eliminate, but may facilitate the removal of residual biofilms, is that it would complement – rather than substitute for – the well-accepted mechanical removal and chemical cleansers used in clinics today.

4.3 Biocompatibility and the Effect of Hydroxyapatite

Silver embodies the classic double-edged sword: toxicity. The same agent that is antibacterial can be toxic to the host cell. The acquired evidence suggests that silver-only chitosan was more effective at inducing a drop in viability and a rise in LDH activity, while the composite was not, thus supporting hypothesis H3. This is in line with the outcome of Salaie et al. (2020), where combined silver and nano-hydroxyapatite led to healthier osteoblasts than silver alone. Notably also, Haugen et al. (2022) noted that slower silver release is more conducive to cell viability. In the present work, the composite released silver at

a slower rate (lowerkH), and had a hydrophilic, nanostructured calcium-phosphate substrate, both of which might help with cellular attachment; the former being a kinetic argument, and the latter being about surface chemistry, and our current experiment cannot tease out these two factors. A similar study of a silver-containing coating on nickel-titanium had also found a beneficial effect both in terms of corrosion and on fibroblasts (Srimaneepong et al., 2020), and Camargo et al. (2021) attempted a similar task with titanium. Altogether, the literature on the matter backs up silver layering over calcium phosphate rather than bare silver.

4.4 Comparison with published work

Table 12. Selected published studies related to the present work.

Study	Material / coating	Main finding relevant here
Oróstica et al. (2024)	Cu-coated CoCr (PVD), multispecies biofilm	Ecorr −0.144 V vs −0.252 V (uncoated) after 15 d with biofilm
Łosiewicz et al. (2023)	Chitosan-Ag on CoCrMo (EPD)	≈1.9 wt% Ag; proposed as antibacterial coating (0.9% NaCl, 37 °C)
Salaie et al. (2020)	Ag + nHA / mHA on Ti6Al4V	Osteoblasts healthier on Ag + nHA than on Ag or Ag + mHA
Haugen et al. (2022)	Review: Ag nanoparticles on Ti implants	Slower Ag release raises cell viability and proliferation
Sakurai et al. (2025)	SLM / EBM / cast Co-Cr, acidic saline	AM < 7 μg cm^{-2} vs cast 42 μg cm^{-2}; all < 200 μg cm^{-2} (ISO 22674)
Bajt Leban et al. (2023)	SLM vs milled CoCr in artificial saliva	Highest ion release in lactic acid despite best PDP result
Presotto et al. (2021)	Cast, milled and SLM Co-Cr	SLM had higher R_p, E_{corr} and E_{pit}
Raile et al. (2025)	Cleansers on Co-Cr biofilm	Lower efficacy against multispecies than mono-species biofilm

4.5 Clinical Relevance

If an RPD prosthesis is worn, the coating will probably be confined to all the covered RPD framework surfaces that will contact with the salivary and plaque. On the other hand, interfaces involving the ceramics and resin should be treated individually. For a coated framework, undercoating may minimize the contact of metal ions with the tissues, plaque accumulation of candida and bacteria and also minimize the injury to neighboring gingiva, which rubs against the RPD clasp and connector. In contrast, the coating should be restricted to the unveneered surfaces for a tooth-supported metal-ceramic crown, as the organic coatings usually do not survive the porcelain firing.

4.6 Future Work

Some areas for future studies that are outlined will involve substitution of measured data for the either/or dummy data, a study using printed framework geometry and cast/milled alloys, as well as wear, brushing, cleaner testing, and thermo mechanical aging. The exposure studies will have to include saliva with protein that is flowed dynamically, along with either a stable or dynamic multispecies biofilm. Examination of immunologic and genotoxic endpoints would be recommended, and, if consistent, a controlled clinical study on silver-containing RPD framework coating might be the next step.

5. CONCLUSIONS

Within the set design specifications, chitosan-based coatings deposited by electrophoresis achieved corrosion current density and metal-ion release retardation from SLM Co-Cr-Mo alloy, with the greatest reduction under acidic conditions. Silver imparted antibacterial and anti-biofilm properties, however was found to promote a reduction in fibroblast viability when tested in isolation. The chitosan-nano-hydroxyapatite-silver composite exhibited excellent corrosion protection and known broad spectrum antibacteriality as well as sustained biocompatibility with gingival fibroblasts, with a slower release rate of silver present compared to a pure silver layer. The findings can be transposed within the design conditions laid out, however

must be substantiated with measured data and ageing conditions relevant to clinical application before any translational implications can be drawn.

REFERENCES

[1] Bajt Leban, M., Kurnik, M., Kopač, I., Klug Jovičević, M., Podgornik, B., & Kosec, T. (2023). Differences between 3-D printed and traditionally milled CoCr dental alloy from casted block in oral environment. *Electrochimica Acta, 445*, 142066. https://doi.org/10.1016/j.electacta.2023.142066

[2] Camargo, S. E. A., Roy, T., Xia, X., Fares, C., Hsu, S., Ren, F., Clark, A. E., Neal, D., & Esquivel-Upshaw, J. F. (2021). Novel coatings to minimize corrosion of titanium in oral biofilm. *Materials, 14*(2), 342. https://doi.org/10.3390/ma14020342

[3] Fratila, A., Jimenez-Marcos, C., Mirza-Rosca, J. C., & Saceleanu, A. (2023). Mechanical properties and biocompatibility of various cobalt chromium dental alloys. *Materials Chemistry and Physics, 304*, 127867. https://doi.org/10.1016/j.matchemphys.2023.127867

[4] Grosgogeat, B., Vaicelyte, A., Gauthier, R., Janssen, C., & Le Borgne, M. (2022). Toxicological risks of the cobalt-chromium alloys in dentistry: A systematic review. *Materials, 15*(17), 5801. https://doi.org/10.3390/ma15175801

[5] Haugen, H. J., Makhtari, S., Ahmadi, S., & Hussain, B. (2022). The antibacterial and cytotoxic effects of silver nanoparticles coated titanium implants: A narrative review. *Materials, 15*(14), 5025. https://doi.org/10.3390/ma15145025

[6] Kajima, Y., Takaichi, A., Kittikundecha, N., Htat, H. L., Cho, H. H. W., Tsutsumi, Y., Hanawa, T., Wakabayashi, N., & Yoneyama, T. (2021). Reduction in anisotropic response of corrosion properties of selective laser melted Co-Cr-Mo alloys by post-heat treatment. *Dental Materials, 37*, e98–e108. https://doi.org/10.1016/j.dental.2020.10.020

[7] Łosiewicz, B., Osak, P., Kubisztal, J., & Górka-Kulikowska, K. (2023). Effect of artificial saliva modification on the corrosion resistance and electronic properties of Bego Wirobond® C dental alloys. *Applied Sciences, 13*(22), 12185. https://doi.org/10.3390/app132212185

[8] Łosiewicz, B., Osak, P., & Kubisztal, J. (2023). The effect of a composite chitosan-silver(I) ion coating on the corrosion resistance of the cobalt-chromium-molybdenum alloy in saline solution. *Progress on Chemistry and Application of Chitin and its Derivatives, 28*, 75–88. https://searchworks.jioinstitute.edu.in/articles/edb__173616255

[9] Oróstica, N., Montoya, L. F., Muñoz, C., Jaramillo, A. F., Rojas, D., Medina-Muñoz, C., Sánchez-Sanhueza, G., & Melendrez, M. F. (2024). Multi-species biofilm interactions and their impact on the biocorrosion of copper-coated CoCr alloys in dental application. *Coatings, 14*(7), 861. https://doi.org/10.3390/coatings14070861

[10] Presotto, A. G. C., Cordeiro, J. M., Presotto, J. G. C., Rangel, E. C., da Cruz, N. C., Landers, R., Barão, V. A. R., & Mesquita, M. F. (2021). Feasibility of 3D printed Co–Cr alloy for dental prostheses applications. *Journal of Alloys and Compounds, 862*, 158171. https://doi.org/10.1016/j.jallcom.2020.158171

[11] Raile, P. N., Curylofo, P. A., Oliveira, V. de C., Macedo, A. P., Vasconcelos, G. L. L., Paranhos, H. F. O., & Pagnano, V. O. (2025). Challenges in defining an efficient cleansing protocol against mono- and multi-species biofilms on a cobalt-chromium alloy surface. *Dental and Medical Problems, 62*(4), 711–719. https://doi.org/10.17219/dmp/170920

[12] Sakurai, N., Sawada, T., Kuwajima, Y., Yamanaka, K., Nomura, N., Kasahara, M., Chiba, A., Satoh, K., & Takemoto, S. (2025). Metallic ion release behaviors from cobalt–chromium alloys fabricated by additive manufacturing with mechanical grinding in an acidic saline solution. *Materials, 18*(2), 432. https://doi.org/10.3390/ma18020432

[13] Şahin, M., Ünalan, F., & Mutlu, İ. (2022). Corrosion, ion release, and surface hardness of Ti-6Al-4V and cobalt-chromium alloys produced by CAD-CAM milling and laser sintering. *The Journal of Prosthetic Dentistry, 128*(3). https://doi.org/10.1016/j.prosdent.2022.06.011

[14] Salaie, R. N., Besinis, A., Le, H., Tredwin, C., & Handy, R. D. (2020). The biocompatibility of silver and nanohydroxyapatite coatings on titanium dental implants with human primary osteoblast cells. *Materials Science and Engineering: C, 107*, 110210. https://doi.org/10.1016/j.msec.2019.110210

[15] Srimaneepong, V., Rokaya, D., Thunyakitpisal, P., Qin, J., & Saengkiettiyut, K. (2020). Corrosion resistance of graphene oxide/silver coatings on Ni-Ti alloy and expression of IL-6 and IL-8 in human oral fibroblasts. *Scientific Reports, 10*, 3247. https://doi.org/10.1038/s41598-020-60070-x

[16] Stewart, P. S., & Bjarnsholt, T. (2020). Risk factors for chronic biofilm-related infection associated with implanted medical devices. *Clinical Microbiology and Infection, 26*(8), 1034–1038. https://doi.org/10.1016/j.cmi.2020.02.027

[17] Tomova, Z., Vlahova, A., Stoeva, I., Zhekov, Y., & Vasileva, E. (2022). Metal ion emission and corrosion resistance of 3D-printed dental alloy. *Open Access Macedonian Journal of Medical Sciences, 10*(D), 143–147. https://doi.org/10.3889/oamjms.2022.8577

[18] Vasylyev, M. O., Mordyuk, B. M., Voloshko, S. M., & Gurin, P. O. (2025). Physiological corrosion and ion release in dental Co–Cr–Mo alloys fabricated using additive manufacturing. *Progress in Physics of Metals, 26*(1), 120–145. https://doi.org/10.15407/ufm.26.01.124